Nonreciprocity in Photon Pair Correlations of Classically Reciprocal Systems

Austin Graf,[1,2] Steven D. Rogers,[3] Jeremy Staffa,[1,2] Usman A. Javid,[1,2] Dana H. Griffith,[4] and Qiang Lin[1,2,5]
[1]Institute of Optics, University of Rochester, Rochester, New York 14627, USA
[2]Center for Coherence and Quantum Optics, University of Rochester, Rochester, New York 14627, USA
[3]John Hopkins University, Applied Physics Laboratory, Laurel, Maryland 20723, USA
[4]Department of Physics, Wellesley College, Wellesley, Massachusetts 02841, USA
[5]Department of Electrical and Computer Engineering, University of Rochester, Rochester, New York 14627, USA

(Received 13 July 2021; accepted 6 April 2022; published 27 May 2022)

Nonreciprocal optical systems have found many applications altering the linear transmission of light as a function of its propagation direction. Here, we consider a new class of nonreciprocity which appears in photon pair correlations and not in linear transmission. We experimentally demonstrate and theoretically verify this nonreciprocity in the second-order coherence functions of photon pairs produced by spontaneous four-wave mixing in a silicon microdisk. Reversal of the pump propagation direction can result in substantial extinction of the coherence functions without altering pump transmission.

DOI: 10.1103/PhysRevLett.128.213605

Nonreciprocal optical systems, which exhibit a change in transmission upon reversing the propagation of an input field, have generated great interest in classical electromagnetism. Many nonreciprocal systems have been achieved with magnetic biasing [1], while others have relied on dynamic modulation [2–4]. Optical nonlinearity has also been leveraged to induce nonreciprocity, especially in chip-scale systems [5–9]. These nonreciprocal systems form the foundation of optical isolation, which has proven vital to laser operations [10,11]. Recently, nonreciprocity has been extended to lasing itself [12], and even been explored in quantum systems to achieve single-photon routing and isolation [13–15], design photon blockades [16,17], and envision one-way entanglement [18]. Recent work has additionally investigated the relationship between quantum correlations and nonreciprocity [15–19], however, the nonreciprocity of quantum correlations in a classically reciprocal system has not yet been fully explored or experimentally demonstrated.

In classical electromagnetism, the change in the ratio between transmitted and incoming fields that occurs upon swapping sources with detectors determines the extent of a system's nonreciprocity [1]. Here, we introduce a new class of nonreciprocity, which does not appear in the linear transmission of light, but rather in the quantum measurement of field coherence. Specifically, in a nonlinear system operating in the single-photon regime, nonreciprocity emerges in the second-order coherence function between quantum optical fields.

We begin to explore the aforementioned nonreciprocity by considering first an optical microdisk with a single scatterer on its surface, shown in Fig. 1(a). Laser light is coupled into the cavity in one of two possible propagation directions via port 1 or port 2, exciting a copropagating whispering-gallery mode (WGM). The single scatterer couples the clockwise-propagating and counter-clockwise-propagating WGMs as light scatters between the modes. The position of the scatterer introduces a crucial asymmetry between ports, creating a dependence of the relative phase between WGMs on the laser light's entry port.

In practice, the disk's surface is not smooth but instead possesses nanoscale roughness, as in Fig. 1(b). The asymmetrical distribution of the surface roughness combines with its subwavelength scale to create a system analogous to that of the smooth microdisk with a single scatterer in Fig. 1(a). Scattering-induced coupling again arises between counterpropagating WGMs. With scattering populating both WGMs and breaking their degeneracy, standing wave eigenmodes such as those in Fig. 1(b) form in the microdisk. The asymmetry observed in the case of the single scatterer persists in the presence of a distributed scatterer like nanoscale surface roughness. That phase asymmetry is now most easily visualized in the standing wave mode pattern, fixed in place by the surface roughness.

The observed phase asymmetry has no effect on the linear optical response of the system. Figure 1(c) shows that there is no change in the transmission when the laser light's input direction is changed. However, if the microdisk additionally exhibits resonantly enhanced third-order ($\chi^{(3)}$) nonlinearity, the laser light may act as a pump to generate pairs of signal and idler photons by spontaneous four-wave mixing (SFWM) [20–22], and nonreciprocity can be observed. Figure 1(d) shows the nonlinear process in the frequency domain, with each of the standing wave pump modes (green) populated by scattering-induced coupling at eigenfrequencies $\omega_p^{\pm} = \omega_p \pm |\beta|$. Here, the central resonance frequency is given by ω_p while $|\beta|$

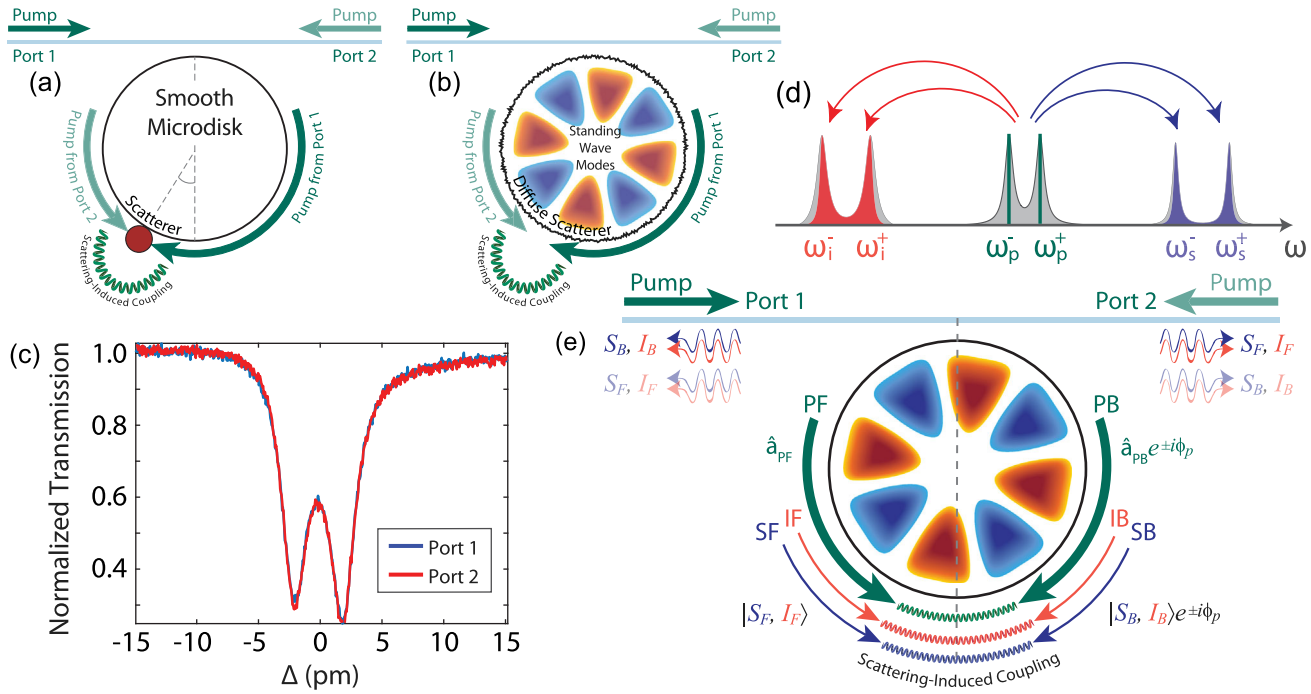

FIG. 1. Nonreciprocity arises in photon pairs generated by cavity-enhanced spontaneous four-wave mixing (SFWM) via coupled whispering-gallery modes (WGMs). (a) A depiction of a smooth silicon microdisk with a single surface scatterer. Pump laser light (green) is introduced at port 1 and evanescently coupled into the microdisk, exciting a forward-propagating WGM. The scatterer couples this mode to a backward-propagating WGM. If the device were instead pumped from port 2 (translucent green), the backward-propagating WGM would be excited and light could scatter to the forward-propagating WGM. The position of the scatterer crucially affects the relative phase between WGMs in each pumping scenario. (b) A depiction of a rough silicon microdisk. Nanoscale surface roughness acts as a distributed scatterer, coupling WGMs and creating standing wave eigenmodes (blue and orange). (c) The experimental cavity transmission of the pump doublet resonance for a pump field introduced at port 1 (blue) and at port 2 (red), which closely match. (d) A frequency domain representation of SFWM in the silicon microdisk showing several biphoton creation pathways. (e) SFWM in a silicon microdisk with scattering-induced coupling. Generated signal and idler photons may coherently scatter between clockwise- and counterclockwise-propagating modes before exiting the device either forward- or backward-propagating relative to the input pump field. The phase relationship between pump modes and generated biphoton states depends on pump field's initial propagation direction.

denotes the scattering rate, or equivalently half of the doublet resonance splitting [23,24]. If nanoscale surface roughness likewise induces splitting at the signal (red) and idler (blue) resonance frequencies, a quantum interference arises between SFWM biphoton creation pathways, an interference that critically depends upon the pump field's incoming propagation direction.

The system in Fig. 1(e) shows how modal coupling at all three (pump, signal, and idler) resonances affects the nonlinear generation of signal and idler photon pairs. Modal coupling dramatically alters the photons' dynamics. Pump light undergoing resonantly enhanced SFWM will always produce copropagating photon pairs to conserve momentum. However, in the presence of modal coupling, these photons can coherently scatter between clockwise- and counterclockwise-propagating WGMs. With respect to the WGMs, this coherent scattering creates a time-evolving path entanglement within the cavity, as the propagation direction of either photon in an entangled pair oscillates via scattering. Oscillations in propagation direction persist until each photon exits the cavity in either the same direction as the input pump (forward) or the opposite direction (backward).

Each signal and idler photon exits the optical cavity probabilistically, at a rate governed by the cavity quality factor. If the signal exits the cavity first, then the idler is free to coherently scatter within the optical cavity. This coherent scattering alters the idler propagation direction correlated with the signal photon's exit direction. An illustrative example considers the situation in which the signal and idler are created propagating in the clockwise direction, and the signal exits the cavity in the forward direction while the idler remains in the cavity. The continued scattering of the idler in the cavity will cause this forward-propagating signal photon to oscillate between correlation with a clockwise-propagating idler and correlation with a counterclockwise-propagating idler until the idler leaves the cavity. The cross-correlation of the photon pair is a function of the difference in emission time between the signal and idler photons, $\tau \equiv t_s - t_i$. As such, oscillations appear in this

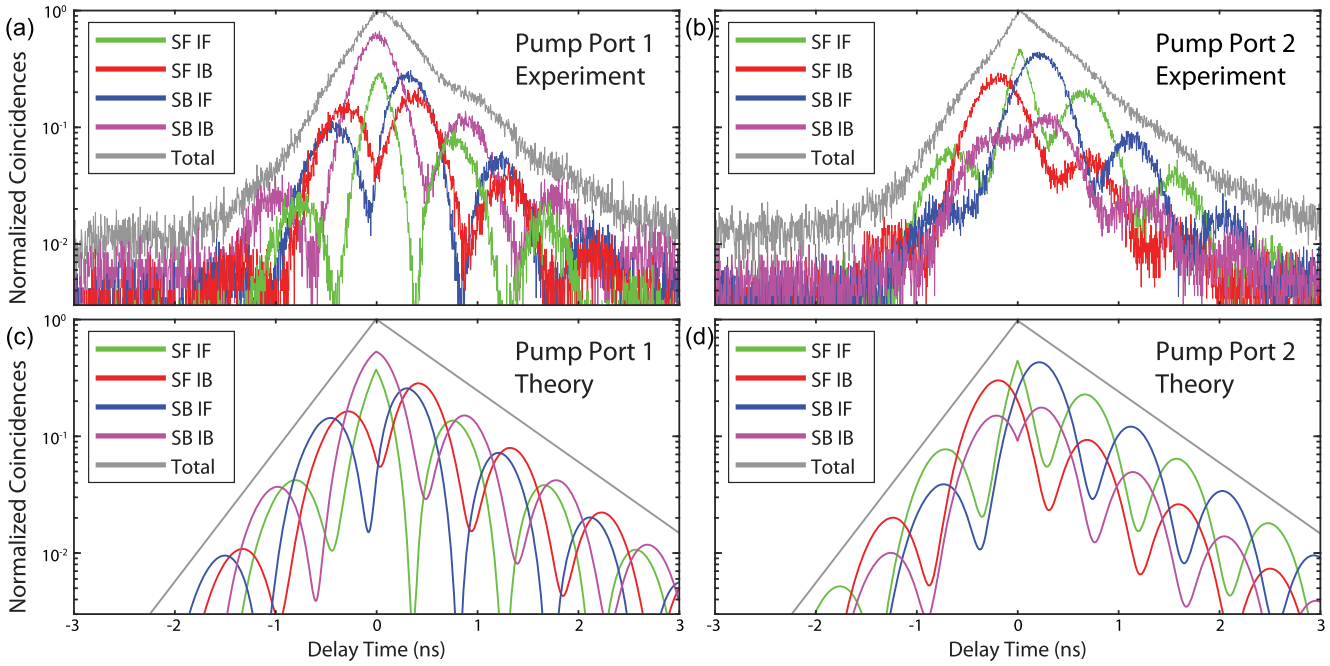

FIG. 2. Normalized second-order biphoton coherence functions. (a) and (b) Measured coincidences are plotted as a function of the difference in the detection times of the signal and idler photons produced by a pump input at port 1 (a) and port 2 (b) for all possible biphoton path configurations: signal-forward and idler-forward (SF IF), signal-forward and idler-backward (SF IB), signal-backward and idler-forward (SB IF), and signal-backward and idler-backward (SB IB). The sum of coherence functions for all four path configurations gives the total coherence function, and all coherence functions are normalized to the maximum of the respective total coherence function. (c) and (d) The theoretically obtained coherence functions corresponding to pump port 1 and pump port 2, respectively.

biphoton coherence function, with an oscillation rate equal to the scattering rate $|\beta|$. These oscillations can equivalently be described in the frequency domain as a beating between two signal (idler) eigenmodes, with the beat frequency given by half the mode splitting, again giving $|\beta|$.

The oscillations are evident in the biphoton coherence functions for four possible pairs of propagation directions: signal-forward and idler-forward (SF IF), signal-forward and idler-backward (SF IB), signal-backward and idler-forward (SB IF), and signal-backward and idler-backward (SB IB). Summing these four functions yields the exponential decay envelope one would expect from a cavity in which no modal coupling is present, verifying conservation of total probability. For a pair of signal and idler photon paths, denoted $j = f,\ b$ and $k = f,\ b$ respectively, the probability that the signal photon arrives at time t_{sj} and the idler photon at time t_{ik} is given by [25]

$$p(t_{sj}, t_{ik}) = Ne^{-\Gamma_{tm}|\tau_{jk}|}|\zeta_m^{jk}\cos(\beta_m\tau_{jk}) + \eta_m^{jk}\sin(\beta_m\tau_{jk})|^2. \tag{1}$$

The subscript $m = s$ for $t_{sj} > t_{ik}$ and i for $t_{sj} < t_{ik}$. The total decay rate Γ_{tm} is consequently determined from either the signal or idler decay rate, depending on the value of m. The complex scattering rate β_m likewise differs between the signal and idler, and it may be written $\beta_m = |\beta_m|e^{i\phi_m}$ where ϕ_m is the phase accrued upon scattering. The normalization coefficient N is determined by parameters of the device. Meanwhile, ζ_m^{jk} and η_m^{jk} are functions of the energy and relative phase of the clockwise- and counterclockwise-propagating intracavity pump modes shown in Fig. 1.

The complex amplitude of these intracavity pump fields can be found as a function of the laser detuning from resonance Δ by solving the coupled-mode equations in the steady state. For an input field b_1 introduced at port 1, the forward and backward propagating fields, relative to the pump direction, are

$$a_f(\Delta) = \kappa(\Delta)(i\Delta - \Gamma_{tp}/2)b_1, \tag{2}$$

$$a_b(\Delta) = \kappa(\Delta)(-i|\beta_p|e^{-i\phi_p})b_1, \tag{3}$$

where $\kappa(\Delta)$ depends upon the cavity decay rate and the modal scattering rate. Pumping at port 2 with field b_2, the complex mode amplitudes are instead

$$a_f(\Delta) = \kappa(\Delta)(i\Delta - \Gamma_{tp}/2)b_2, \tag{4}$$

$$a_b(\Delta) = \kappa(\Delta)(-i|\beta_p|e^{i\phi_p})b_2. \tag{5}$$

Thus pumping at the second port instead of the first alters the relative phase between intracavity modes by $2\phi_p$, twice

the pump scattering phase. The phase difference will influence the quantum interference occurring within the microresonator and induce corresponding phase shifts in the second-order biphoton cross-correlations. The joint spectral amplitude of the generated biphotons is unaffected.

A silicon microdisk of radius 4.5 μm and thickness 260 nm is used to experimentally verify that nonreciprocity arises in the second-order cross-correlation. The SFWM process harnesses three adjacent quasi-transverse-magnetic (quasi-TM) doublet modes at wavelengths 1532, 1551, and 1569 nm, and average intrinsic quality factors over 8×10^5. The magnitude of the complex scattering rate is 0.55, 0.26, and 0.48 GHz for signal, pump, and idler modes respectively.

Pump light is evanescently coupled into the device via either port 1 or port 2 of the tapered optical fiber. Wavelength-division multiplexers separate signal, idler, and pump photons. Optical switches allow for control over which propagation pathway of emitted signal and idler photons are detected with superconducting nanowire single-photon detectors. In this way all combinations of propagation directions for signal and idler photon pairs can be measured. A time-correlated single-photon counter is used to acquire the detection times of the signal and idler photons. A schematic of the experimental setup can be found in Supplemental Material [26].

Figures 2(a) and 2(b) contrast the biphoton correlation functions that arise in the presence of a pump laser from port 1 with those generated by a pump laser from port 2. Normalized biphoton coincidence counts collected over a three minute data acquisition time are plotted against delay time τ. A dramatic phase shift can be observed in the correlations' oscillations upon reversing the pump direction. Theory derived from the coupled-mode equations and Heisenberg-Langevin equations [27] predicts this phase shift. Figures 2(c) and 2(d) demonstrate the correspondence with theory, respectively for inputs at pump port 1 and pump port 2. In all cases, the theory accurately replicates the experimentally observed system behavior. The differences that are present between experimental and theoretical biphoton coherence functions are likely due to the application of the coupled-mode equations. To focus on the underlying nonreciprocal physics of the system, we approximate the standing wave modes of each resonance as having identical loss rates, but in general they exhibit unique loss rates [28].

Further evidence verifying the mechanism of the biphoton coherence functions' phase shifts can be provided by examining a second device, one which does not exhibit coupling between pump modes. Such a device, the resonance structure of which is presented in Fig. 3(a), would still show oscillations in the biphoton coherence function as a result of modal coupling in the signal and idler modes, but these oscillations would not change with a change in pump

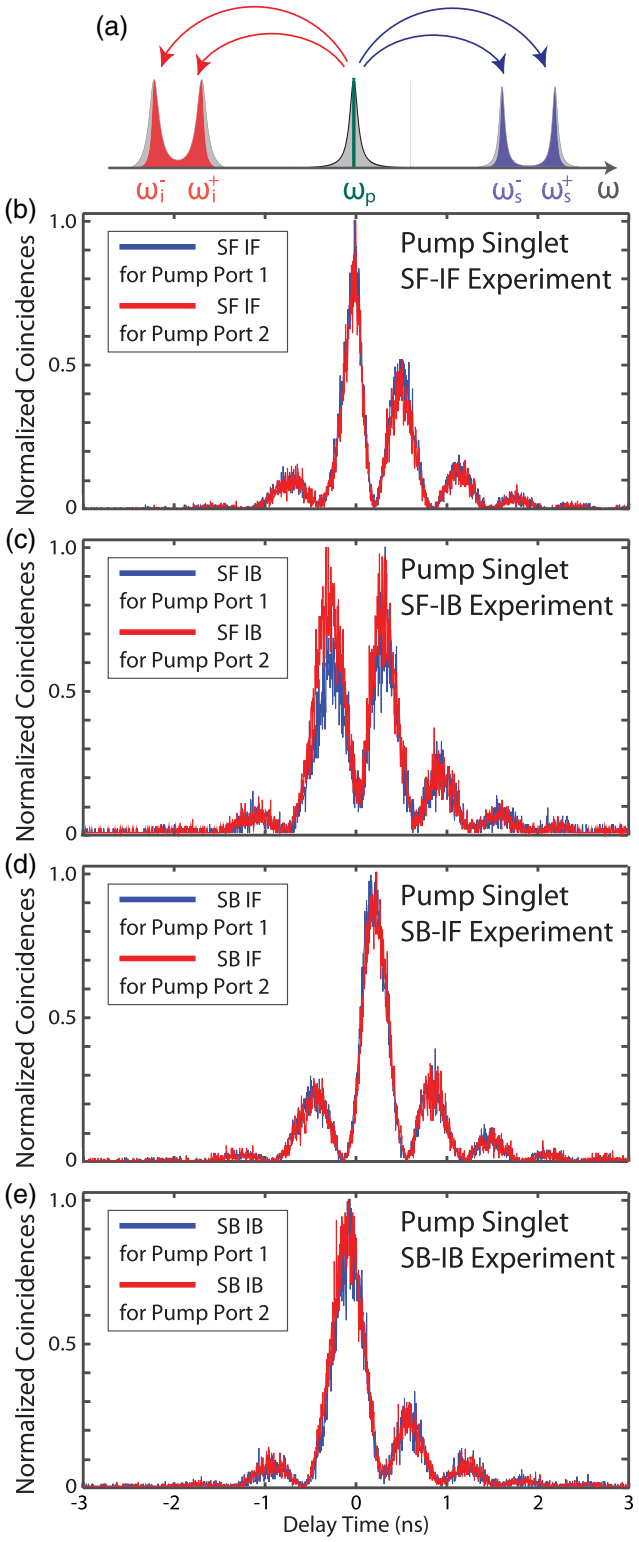

FIG. 3. Description of a microdisk with a singlet pump mode. (a) A frequency domain picture of SFWM with a singlet pump. (b) Second-order coherence function (normalized to its maximum) for (b) SF IF, (c) SF IB, (d) SB IF, and (e) SB IB biphoton path configurations from a microdisk with a singlet pump mode.

input direction. This implies that the doublet nature of the pump mode is indeed vital to the observed phase shift.

The variation in nanoscale surface roughness between fabricated devices allowed us to test such a device, and the results are displayed in Figs. 3(b)–3(e). With a radius of 4.4 μm and a thickness of 260 nm, the device exhibits doublet modes at 1531 and 1567 nm with quality factors over 8×10^5 and complex scattering rates of 0.80 and 0.62 GHz, and a singlet mode at 1549 nm with a quality factor of 4.1×10^5. For all four biphoton path configurations, there is no change observed in the second-order coherence function upon changing pump direction. This verifies that the coupling between counterpropagating pump modes is requisite to the nonreciprocity observed in the second-order biphoton coherence functions.

The silicon microdisk's intrinsic scattering phase primarily determines the extent of the phase shift that occurs in the biphoton coherence functions when the input pump port is changed. In the described experiment, the coupling mechanism between counterpropagating modes is Rayleigh scattering mediated by the device's nanoscale surface roughness, and the associated scattering phase is not tuned. Importantly though, this phase can be tuned for the desired application by modulating the device's radius during fabrication [29], or, if reconfigurability is required, by applying an external scattering probe [30,31].

The degree of the phase shift, and likewise the extinction ratio, can also be tuned by varying the pump laser wavelength. Detuning the pump laser from resonance changes the relative power and relative phase between counterpropagating pump fields in the device, which can shift peaks to nulls (and nulls to peaks) in the second-order biphoton coherence functions.

The extent of the device's tunability enhances its utility. As a source, it provides highly configurable path-entangled photon pairs. Active device tuning such as phase modulation of the pump laser or mechanical modulation of the microdisk allow even greater control over the intercavity quantum state and the device's nonreciprocity. With these techniques, the nonreciprocity can be continuously tuned through its full range. Expanding the system to multiple devices, this active approach can yield high-dimensional and multipartite quantum states [32,33]. The system's nonreciprocity provides a means of phase control over generated quantum states, independent of detuning and thus bypassing the limitations of thermal locking [34].

The device additionally provides an avenue toward nonreciprocal quantum processing. Because the nonreciprocity arises from doublet splitting, it can be harnessed from splitting in the signal or idler mode via single-photon stimulated SFWM [35,36]. This could in turn be applied to the routing of discrete multipartite quantum states [36,37] or nonreciprocal quantum state manipulation and control [38]. The device could also be operated as a phase-sensitive optical parametric oscillator to realize nonreciprocal squeezing [39,40].

Beyond its applicability, the silicon microdisk system illustrates a new class of nonreciprocity in the second-order coherence functions of its nonlinearly created photon pairs. The complete experimental and theoretical description of such a system provides deeper insight and intuition into the quantum behavior of nonlinear nonreciprocal systems. Moreover, the understanding developed by the theoretical and experimental demonstration of nonreciprocity in biphoton coherence functions can be applied to any system regardless of platform, inviting the possibility of new developments in nonreciprocal quantum structures.

This work is supported in part by National Science Foundation (NSF) under Grants No. EFMA-1641099, No. ECCS-1810169, and No. ECCS-1842691. The work was performed in part at the Cornell NanoScale Facility, a member of the National Nanotechnology Coordinated Infrastructure (NNCI), which is supported by the National Science Foundation (Grant No. NNCI-2025233).

[1] C. Caloz, A. Alù, S. Tretyakov, D. Sounas, K. Achouri, and Z.-L. Deck-Léger, Phys. Rev. Applied **10**, 047001 (2018).
[2] D. L. Sounas and A. Alù, Nat. Photonics **11**, 774 (2017).
[3] E. Verhagen and A. Alù, Nat. Phys. **13**, 922 (2017).
[4] M.-A. Miri, F. Ruesink, E. Verhagen, and A. Alù, Phys. Rev. Applied **7**, 064014 (2017).
[5] F. Song, Z. Wang, E. Li, Z. Huang, B. Yu, and B. Shi, Appl. Phys. Lett. **119**, 024101 (2021).
[6] S. Hua, J. Wen, X. Jiang, Q. Hua, L. Jiang, and M. Xiao, Nat. Commun. **7**, 13657 (2016).
[7] L. D. Bino, J. M. Silver, M. T. M. Woodley, S. L. Stebbings, X. Zhao, and P. Del'Haye, Optica **5**, 279 (2018).
[8] X. Zhou, Y. Wang, D. Leykam, and Y. D. Chong, New J. Phys. **19**, 095002 (2017).
[9] K. Wang, S. Gao, Y. Wang, A. Nirmalathas, C. Lim, K. Alameh, and E. Skafidas, IEEE Photonics Technol. Lett. **28**, 1739 (2016).
[10] D. Jalas, A. Petrov, M. Eich, W. Freude, S. Fan, Z. Yu, R. Baets, M. Popović, A. Melloni, J. D. Joannopoulos, M. Vanwolleghem, C. R. Doerr, and H. Renner, Nat. Photonics **7**, 579 (2013).
[11] L. J. Aplet and J. W. Carson, Appl. Opt. **3**, 544 (1964).
[12] B. Bahari, A. Ndao, F. Vallini, A. El Amili, Y. Fainman, and B. Kanté, Science **358**, 636 (2017).
[13] C. Gonzalez-Ballestero, E. Moreno, F. J. Garcia-Vidal, and A. Gonzalez-Tudela, Phys. Rev. A **94**, 063817 (2016).
[14] Y. You, Y. Hu, G. Lin, Y. Qi, Y. Niu, and S. Gong, Phys. Rev. A **103**, 063706 (2021).
[15] A. Rosario Hamann, C. Müller, M. Jerger, M. Zanner, J. Combes, M. Pletyukhov, M. Weides, T. M. Stace, and A. Fedorov, Phys. Rev. Lett. **121**, 123601 (2018).
[16] X. Xu, Y. Zhao, H. Wang, H. Jing, and A. Chen, Photonics Res. **8**, 143 (2020).
[17] R. Huang, A. Miranowicz, J.-Q. Liao, F. Nori, and H. Jing, Phys. Rev. Lett. **121**, 153601 (2018).

[18] Y.-F. Jiao, S.-D. Zhang, Y.-L. Zhang, A. Miranowicz, L.-M. Kuang, and H. Jing, Phys. Rev. Lett. **125**, 143605 (2020).
[19] X. Lu, W. Cao, W. Yi, H. Shen, and Y. Xiao, Phys. Rev. Lett. **126**, 223603 (2021).
[20] R. W. Boyd, *Nonlinear Optics*, 3rd ed. (Academic Press, Inc., Orlando, FL, 2008).
[21] L. G. Helt, Z. Yang, M. Liscidini, and J. E. Sipe, Opt. Lett. **35**, 3006 (2010).
[22] S. Clemmen, K. P. Huy, W. Bogaerts, R. G. Baets, P. Emplit, and S. Massar, Opt. Express **17**, 16558 (2009).
[23] D. S. Weiss, V. Sandoghdar, J. Hare, V. Lefèvre-Seguin, J.-M. Raimond, and S. Haroche, Opt. Lett. **20**, 1835 (1995).
[24] A. Mazzei, S. Götzinger, L. de S. Menezes, G. Zumofen, O. Benson, and V. Sandoghdar, Phys. Rev. Lett. **99**, 173603 (2007).
[25] S. D. Rogers, A. Graf, U. A. Javid, and Q. Lin, Commun. Phys. **2**, 95 (2019).
[26] See Supplemental Material at http://link.aps.org/supplemental/10.1103/PhysRevLett.128.213605 for theory and experimental setup.
[27] D. Boyanovsky and D. Jasnow, Phys. Rev. A **96**, 062108 (2017).
[28] Q. Li, A. A. Eftekhar, Z. Xia, and A. Adibi, Phys. Rev. A **88**, 033816 (2013).
[29] X. Lu, S. Rogers, W. C. Jiang, and Q. Lin, Appl. Phys. Lett. **105**, 151104 (2014).
[30] J. Zhu, Şahin Kaya Özdemir, L. He, and L. Yang, Opt. Express **18**, 23535 (2010).
[31] C. Schmidt, M. Liebsch, A. Klein, N. Janunts, A. Chipouline, T. Käsebier, C. Etrich, F. Lederer, E.-B. Kley, A. Tünnermann, and T. Pertsch, Phys. Rev. A **85**, 033827 (2012).
[32] M. Kues, C. Reimer, P. Roztocki, L. R. Cortés, S. Sciara, B. Wetzel, Y. Zhang, A. Cino, S. T. Chu, B. E. Little, D. J. Moss, L. Caspani, J. Azaña, and R. Morandotti, Nature (London) **546**, 622 (2017).
[33] D. Llewellyn, Y. Ding, I. I. Faruque, S. Paesani, D. Bacco, R. Santagati, Y.-J. Qian, Y. Li, Y.-F. Xiao, M. Huber, M. Malik, G. F. Sinclair, X. Zhou, K. Rottwitt, J. L. O'Brien, J. G. Rarity, Q. Gong, L. K. Oxenlowe, J. Wang, and M. G. Thompson, Nat. Phys. **16**, 148 (2020).
[34] X. Jiang and L. Yang, Light **9**, 24 (2020).
[35] Y. Zhang, M. Kues, P. Roztocki, C. Reimer, B. Fischer, B. MacLellan, A. Bisianov, U. Peschel, B. E. Little, S. T. Chu, D. J. Moss, L. Caspani, and R. Morandotti, Laser Photonics Rev. **14**, 2000128 (2020).
[36] S. Dong, X. Yao, W. Zhang, S. Chen, W. Zhang, L. You, Z. Wang, and Y. Huang, ACS Photonics **4**, 746 (2017).
[37] A. Lamas-Linares, J. C. Howell, and D. Bouwmeester, Nature (London) **412**, 887 (2001).
[38] F. De Martini, V. Bužek, F. Sciarrino, and C. Sias, Nature (London) **419**, 815 (2002).
[39] R. Tang, P. S. Devgan, V. S. Grigoryan, P. Kumar, and M. Vasilyev, Opt. Express **16**, 9046 (2008).
[40] L.-A. Wu, M. Xiao, and H. J. Kimble, J. Opt. Soc. Am. B **4**, 1465 (1987).